Materials and Design 160 (2018) 549–556

Contents lists available at ScienceDirect

Materials and Design

journal homepage: www.elsevier.com/locate/matdes

Stochastic continuum model for mycelium-based bio-foam

M.R. Islam [a], G. Tudryn [b], R. Bucinell [c], L. Schadler [d], R.C. Picu [a,*]

[a] Department of Mechanical, Aerospace and Nuclear Engineering, Rensselaer Polytechnic Institute, Troy, NY 12180, USA
[b] Ecovative Design LLC, Green Island, NY 12183
[c] Department of Mechanical Engineering, Union College, Schenectady, NY 12308, USA
[d] Department of Material Science and Engineering, Rensselaer Polytechnic Institute, Troy, NY 12180, USA

HIGHLIGHTS

- Novel biofoam, developed from the root structure (mycelium) of fungi, is characterized under axial compression.
- The material response is highly nonlinear and controlled by microscopic randomness and density variability.
- Mycelium biofoam exhibits strong stress softening and hysteresis under cyclic loading.
- A multiscale model is presented, capturing the microscale structure and mesoscale density fluctuation of the material.

GRAPHICAL ABSTRACT

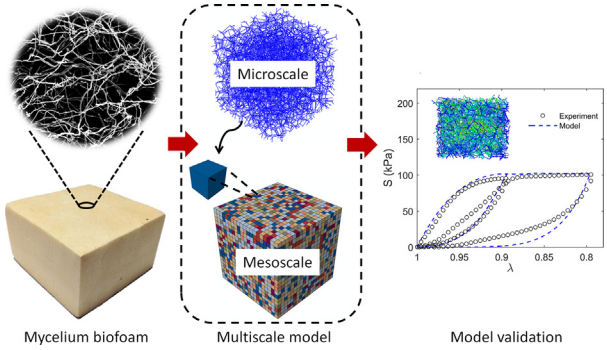

ARTICLE INFO

Article history:
Received 22 May 2018
Received in revised form 22 September 2018
Accepted 27 September 2018
Available online 29 September 2018

Keywords:
Mycelium
Fibrous materials
Mullins effect
Cyclic loading
Constitutive modeling

ABSTRACT

Mycelium, the root structure of fungi, grows naturally as a biodegradable filamentous material. This unique material has highly heterogeneous microstructure with pronounced spatial variability in density and exhibits strongly non-linear mechanical behavior. In this work we explore the material response in compression, under cyclic deformation, and develop an experimentally-validated multiscale model for its mechanical behavior. The deformation localizes in stochastically distributed sub-domains which eventually percolate to form macroscopic bands of high density material. This is reflected in the stress-strain curve as strain softening. Cycling at fixed macroscopic strain leads to deformation history dependence similar to the Mullins effect. To capture this behavior, we use a two-scale model. At the micro-scale, a random fiber network is used, while at the macroscale the spatial density fluctuations are captured using a stochastic continuum model. The density-dependent local constitutive behavior is defined by the microscale model. An empirical damage model is incorporated to account for the experimentally observed cyclic softening behavior of mycelium. The model is further validated by comparison with a separate set of experimental results. The model can be used to explore the effect of mesoscale density fluctuations on the overall mechanical behavior and to design mycelium-based products with desired mechanical performance.

1. Introduction

Mycelium is a sustainable alternative to petroleum-based polymeric materials. It grows naturally as the root structure of fungus and self-organizes as a network of tubular filaments, called hyphae, Fig. 1.

* Corresponding author.
E-mail address: picuc@rpi.edu (R.C. Picu).

https://doi.org/10.1016/j.matdes.2018.09.046
0264-1275/

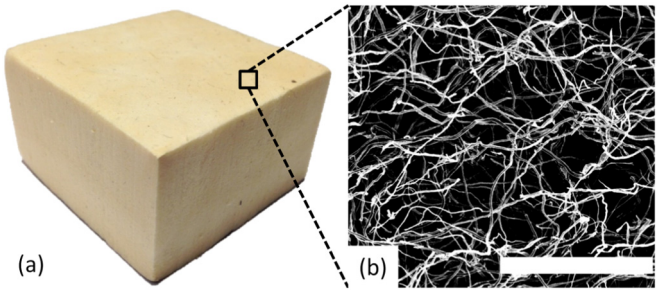

Fig. 1. Illustration of mycelium-based bio-foam: (a) macroscopic structure (50 × 50 × 50 mm) and (b) microstructure of mycelium; scale bar 100 μm.

Mycelium has the potential to emerge as a material of choice for lightweight structures with several advantages such as low density, low production cost, minimal processing energy input and, most importantly, 100% biodegradability. To promote the applications of this novel fungal bio-material, a precise understanding of its deformation behavior is required.

Recent experiments on mycelium indicate that it demonstrates significant non-linear behavior under compression [1]. In particular, mycelium exhibits three distinct regimes under compression, somewhat similar to open cell foams [2]. Linear elastic behavior is observed at small strains. This is controlled by hyphae bending and does not entail significant structural reorganization of the network. A second regime emerges at larger strains, which is associated with fiber buckling and local structural collapse/densification leading to strain stiffening. In the third regime, rapid stiffening is associated, with full compaction and the formation of a large number of inter-fiber contacts. It is observed that the strain distribution is highly heterogeneous due to strong structural disorder and density fluctuations. Deformation localizes at multiple sites which eventually merge into one or multiple bands that percolate through the sample [1].

Mycelium also exhibits significant hysteretic behavior under cyclic compression, including stress softening, or the Mullin's effect, and the occurrence of residual strain, similar to filled and unfilled elastomers [3,4]. When subjected to compressive cycles of constant strain amplitude, the response is softer during reloading compared to the response of the virgin material. This softening diminishes gradually in successive cycles.

The mechanical behavior of mycelium is dictated by the structure of the underlying network and the properties of the constituent fibers – the hyphae. The hypha is a hollow filament and its major structural components are chitin nanofibers, beta-glucans and proteins [5]. Chitin nanofibers form a network which is covalently cross-linked with beta-glucans, and constitutes the structural element of the hypha wall [5,6]. Several researchers studied the mechanical properties of chitin nanofiber-based membranes. Jeffe et al. [7] observed a tensile modulus of 3 GPa and tensile strength of 50 MPa for regenerated chitin membranes. Ifuku et al. [8] extracted chitin nanofiber networks from exoskeletons of crabs and prawns and measured similar values for the modulus (~2.5 GPa) and tensile strength (~45 MPa). Fan et al. [9] reported a tensile modulus of 5 GPa and strength of 140 MPa from chitin nanowhiskers. Mushi et al. [10] observed that properties of the chitin nanofiber network largely depends on the nanofiber volume fraction and the tensile modulus varies from 2.5 to 8.2 GPa for volume fractions ranging from 42% to 78%. The tensile strength varies from 29 to 77 MPa in the same range of volume fractions. Note that the chitin percentage in mycelium is in the range 34 to 68% [11].

In recent years, significant research effort has been devoted to delineate structure-property relations of network-based materials [12]. Several micromechanical models are employed using simplified periodic unit cells or representative volume elements (RVE) of realistic systems to obtain the effective mechanical response. In the small strain regime, network behavior is largely determined by the density, degree of connectivity and the fiber bending-to-axial stiffness ratio. For dense networks with fibers that are relatively stiff in bending, the network undergoes affine deformation. In these conditions the network modulus scales linearly with the density and the fiber axial stiffness. On the other hand, networks of low density, sparse connectivity and/or fibers which are relatively soft in bending, deform in a highly non-affine way. In this case, small strain modulus varies as a power function of the network density (this dependence is quadratic for mycelium [1]) and scales linearly with the fiber bending rigidity.

Network behavior in the collapse/densification regime was also studied using micromechanical models. It is shown [2] that the network softens in this regime due to elastic buckling and/or formation of plastic hinges at fiber-fiber joints. For elastic fibers, the stress-strain curve in this regime has positive slope (much smaller compared to that of the linear regime) which is controlled by the network architecture and structural stochasticity. In particular, a random fibrous network shows larger slope in the collapse/densification regime compared to cellular networks, where fibers are arranged in polyhedral cells [13]. Further, if fibers are elastic-plastic, the network loses stability and shows a more drastic softening behavior with zero or negative stress-strain slope [14].

In contrast to micromechanical models, several phenomenological models were also developed. These consider the network as a continuum material and describe the behavior through empirical constitutive equations without considering microstructural details [15]. Most phenomenological models rely on the hyperelastic model formulation and use suitable forms of the strain energy function to predict experimental observations. A large set of strain energy functional forms are available, including Mooney-Rivlin [16], Arruda-Boyce [17], and Ogden [18] models. Hyperelastic models provide reasonably accurate predictions of the non-linear stress-strain response during compression loading, but cannot capture hysteresis, Mullin's effect and residual strains. To model the stress softening effect, several researchers incorporate additional damage type variables in the hyperelastic model that remain inactive during loading but are activated during unloading based on the maximum strain reached [3,19].

While the above-mentioned microstructurally-detailed models of fibrous materials, as well as other similar works, established the relation between network parameters and its overall properties, they refer to structures with mesoscale homogeneity. Specifically, on scales larger than the size of the respective 'representative volume elements,' the material is considered homogeneous. However, real fibrous materials, including mycelium, exhibit density fluctuations on all scales, up to the macroscopic scale [20]. The effect of mesoscale fluctuations of material properties has been discussed in the literature on stochastic composite materials [21,22], mostly in the context of linear elastic constitutive behavior [23]. Pronounced heterogeneity modifies the global mechanical behavior, promoting softening and localization. Accounting for such mesoscale effects in explicit fiber network models is not feasible since this implies modeling large structures while resolving every fiber in the material. Therefore, a multiscale approach is needed. Developing such representation for mycelium materials is the central objective of the present work.

To this end, we expand our recent work [1] by performing additional experimental characterization of mycelium of different effective densities, and developing a 3D multiscale model that accounts for strain localization and the Mullins effect. An explicit network model is used on the microscale and a stochastic continuum representation is used on the mesoscale. The local constitutive behavior of the continuum is dictated by the local density and the response of the corresponding microscale network model. Ogden's model is used on the continuum scale to represent Mullin's effect observed experimentally. The model is validated by comparison with a separate set of experimental results. The model can be further used to explore the effect of mesoscale heterogeneity on the overall mechanical behavior of the material, and to design the

multiscale structure of mycelium to meet targeted global properties for specific applications.

2. Experimental details and results

The mycelium samples used in this work were provided by Ecovative Design, LLC. The samples were prepared as follows: the mycelium vegetative tissue is first inoculated in a filter patch bag with nutrition (calcium and carbohydrate) and water. After an initial growth phase (around 4 days), the substrate is ground into small pieces to redistribute the growth evenly throughout the material. This step also prevents preferential colonized growth of mycelium in the vicinity of nutrition sites. Next, the material is packed into rectangular molds ($6'' \times 6\Delta'' \times 1''$) and additional nutrition is added to promote further growth. Mycelium is allowed to grow for around six additional days in the molds. As a last step, the samples were heat treated to stop hyphae growth.

Microscopic imaging was carried out to characterize the microstructure of mycelium, using a VERSA 3D Dual Beam Scanning Electron Microscope (SEM). SEM images were processed using ImageJ [24] to evaluate various parameters such as the fiber diameter, segment length, orientation and pore size. The mean hypha diameter, segment length and pore size were 1.3 ± 0.66 μm, 6.5 ± 4.7 μm and 5.8 ± 4.1 μm, respectively. Furthermore, it was observed that fibers (hyphae) have no preferential orientation. The mass density of the samples was also measured to evaluate the effect of density on mechanical properties.

Cuboid specimens of dimensions - 20 mm × 20 mm × 16 mm are cut for compression testing using a bandsaw. An EnduraTec Elf 3200 mechanical testing machine (BOSE, Eden Prairie, MN) with displacement control was used for mechanical testing in ambient conditions (25°C and ~50% relative humidity). A constant strain rate of $6.25 \times 10^{-3}\ s^{-1}$ was used for all tests during both loading and unloading. Cyclic loading tests with no hold/relaxation between cycles were performed under compression.

Fig. 2(a) illustrates the generic stress-strain response of mycelium under compression. The test is performed with a sample of effective density $\rho_s = 34\ kg/m^3$. The stress-strain measures used in this work are the nominal stress (computed as the total applied force divided by the initial cross-sectional area of the sample), S, and the stretch ratio, λ. The response is linear elastic at small strains, with constant Young's modulus E = 1.3 MPa. Starting in the range $0.97 > \lambda > 0.92$ the material undergoes gradual softening due to strain localization and the initiation of collapse band formation. A pronounced hysteretic response is observed upon unloading. Samples of higher density ($\rho_s = 59\ kg/m^3$) exhibit similar behavior (Fig. 2(a)), although the small strain modulus and the stress at the onset of localization are larger. Fig. 2(b) shows the stress-strain curves for five compressive loading-unloading cycles performed at two different maximum strain levels for a sample of density $\rho_s = 59\ kg/m^3$. Unloading is performed immediately after loading, with the same strain rate ($6.25 \times 10^{-3}\ s^{-1}$). Mycelium softens cyclically, i.e. a smaller stress is required in subsequent cycles to compress the material to the same strain level. However, once the strain exceeds the previously imposed maximum strain level, the loading curve converges to what would have been obtained from a monotonic compression of a virgin sample (Fig. 2(b)). Part of these experimental results is used in Section 4 for model calibration, while the reminder of the data set is used for validation.

3. Multiscale model for mycelium

The multiscale model developed for mycelium is presented in this section. At the microscale, we consider representative volume elements of the hyphae network and characterize their mechanical behavior as a function of the effective network density. A hyperelastic model with density-dependent parameters is fitted to these results. This is then used as constitutive representation in a stochastic mesoscale continuum model which accounts for density fluctuations on a scale much larger than that of the microscale network models. Hence, the continuum model is heterogeneous in terms of all parameters of the hyperelastic description, which fluctuate spatially as a function of density. A damage phenomenological model is introduced in the continuum representation in order to capture the Mullins effect (Fig. 2). An alternative to this procedure would be to allow damage (e.g. fiber failure) to evolve on the microscale in each representative volume element and import that information in the upper scale continuum model. We avoid taking this route due to the limited data available at this time about the conditions in which individual hyphae rupture or lose their load carrying capacity.

Fig. 3 shows this procedure schematically. The distribution of mycelium density on the mesoscale has been characterized in our previous work [1]. This distribution is mapped to a histogram of 10 specific density values. Microscale network models, in which each fiber is explicitly represented, are constructed for each of these densities. The average response to uniaxial compression of multiple replicas of a given density is fitted with a hyperelastic model. Further, a stochastic continuum model is constructed and each mesoscale sub-domain is assigned the constitutive model associated with the local density. We present next each of these modeling steps.

3.1. Microscale model

The random fiber network model used at the microscale is a Voronoi network. A set of randomly distributed seed points are used to construct the tessellation of the domain in which the network is defined, and fibers are placed along the edges of the resulting polyhedral cells to obtain a random fiber network. In this algorithm, the network density is

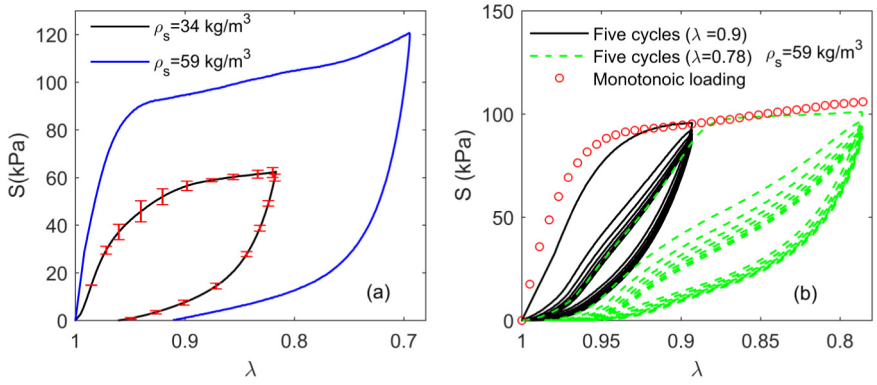

Fig. 2. Experimental stress-strain response of mycelium under compression- (a) single compression cycle for mycelium of densities $\rho_s = 34\ kg/m^3$ and $\rho_s = 59\ kg/m^3$, and (b) five successive compression cycles performed on same sample at two different maximum stretches ($\lambda = 0.9$ and $\lambda = 0.79$ respectively) for a mycelium of density $\rho_s = 59\ kg/m^3$.

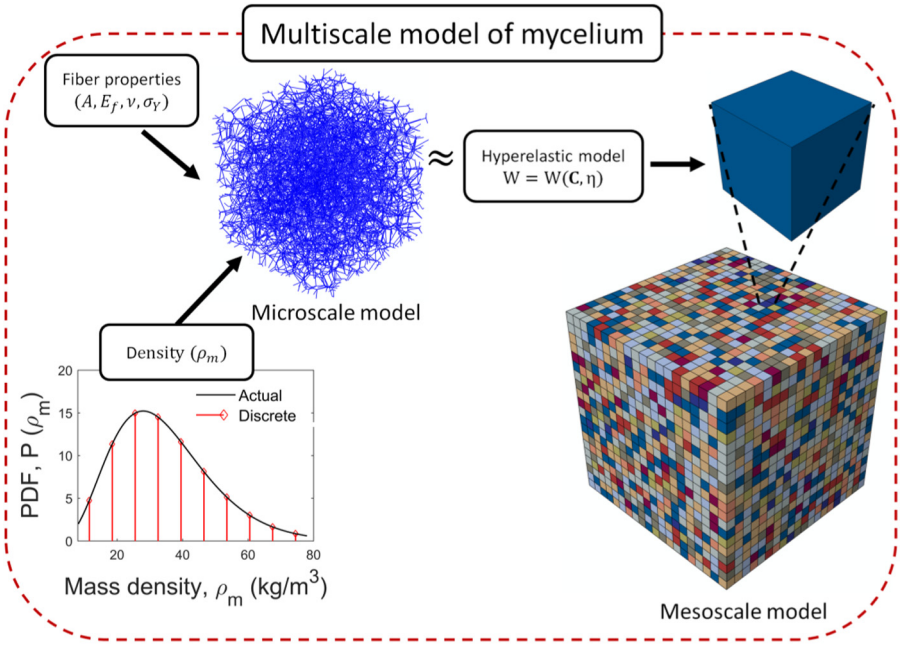

Fig. 3. Schematic representation of the multiscale mycelium model.

controlled by the density of seed points. We adjust the distribution of seed points so as to mimic closely the pore size distribution of mycelium observed microscopically. Fig. 4 compares pore size probability distribution functions of experimental samples and microscale model. It is noted that the experimental pore size distribution corresponds to the two dimensional (2D) projection of mycelium network as observed in SEM images of finite (and known) depth of focus. As such, the pore size of the microscale model was also evaluated for thin sections of same thickness to ensure proper comparison with experimental values.

The network mass density, ρ_m, is defined as:

$$\rho_m = \left(\frac{1}{L^3}\right)\rho_f A \sum_{i=1}^{N} l_i \tag{1}$$

where L is the size of the 3D domain, ρ_f is the density of a hypha wall, A is the cross-section area of a typical tubular hypha, N is the number of filaments in the network and l_i is the length of the ith filament.

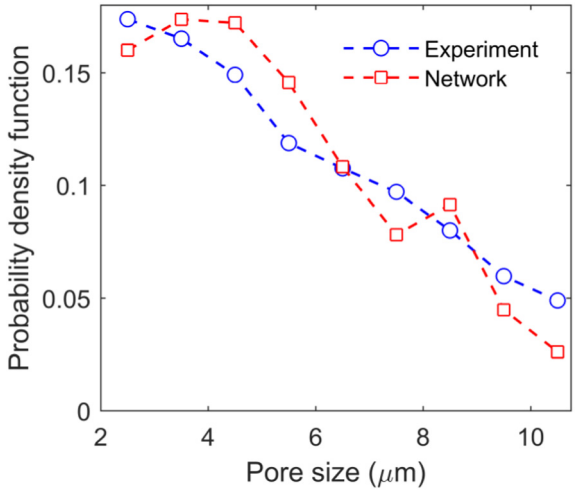

Fig. 4. Comparison of pore size distribution functions for experimental samples and microscale model.

The fiber segment length in the model (l_c) varies from 4 to 8 μm (experimental, $l_c \approx 6.5$ μm) depending on the network density (ρ_m). All filaments in the network model are assumed to have identical cross-section with outer diameter d_0=1.3 μm (experimental, $d_o \approx 1.3$ μm) and wall thickness ($t_w = 100$ nm [5]). The base material of the filament is chitin which has density, $\rho_f = 1430$ kg/m^3. We used an elastic-plastic material model based on literature data for chitin nanofilament networks (the structural constituent of the hypha wall) following ref. [8], with the elastic modulus, Poisson ratio and yield strength as 2.5 GPa, 0.3 and 45 MPa respectively. Beyond the yield point, the material behavior is assumed to follow linear strain hardening with a stiffness ratio of 0.02 between elastic and plastic regime. The generated network is discretized using shear-deformable Timoshenko beams. The minimum element aspect ratio is 5.

Fiber to fiber contact is incorporated using surface based contact constraints using the general contact algorithm in Abaqus [25]. The contact behavior normal to fiber surfaces is implemented with zero penetration condition ('hard' contact algorithm in Abaqus). The relative sliding between fibers is represented as Coulomb friction with a coefficient of friction, $\mu_f = 0.3$, as suggested in refs. [26, 27]. The hypha network is deformed in uniaxial compression by introducing two rigid surfaces at the top and bottom boundaries while imposing equal and opposite displacement boundary conditions on these surfaces. The lateral faces of the model are kept traction free and all other degrees of freedom are free. Finite element simulations are performed using the general purpose finite element solver Abaqus/Explicit (version 6.13-1) [25].

It has been discussed in the literature that fiber networks exhibit strong size effects [28] depending on the fiber elastic properties. Specifically, for fibers which are rather rigid in bending, the scale of homogeneity (i.e. scale at which the response becomes independent of model size) is equal to few fiber segment lengths (l_c). If fibers are soft in bending, which is the case for mycelium, the scale of homogeneity increases gradually as the bending stiffness of filaments decreases. In the current work, a large model size ($L \geq 12 l_c$) is selected to exclude the network size effect.

The compressive stress-strain responses of samples with four representative network densities are illustrated in Fig. 5. At small compressive strains ($\lambda \leq 0.95$), the curves show a linear elastic response where deformation is largely dominated by fiber bending.

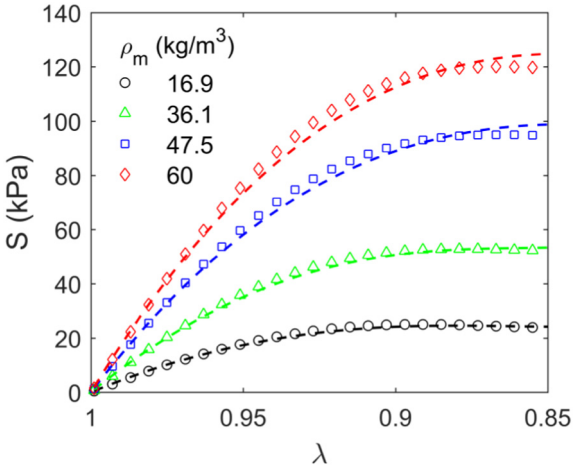

Fig. 5. Stress-strain response of microscale network models of four representative densities under uniaxial compression. The symbols indicate the network response (averaged over three realizations) and the lines represent the fitted hyperelastic constitutive model, Eq. (3) (Section 3.3).

The small strain modulus scales quadratically with density. As the compressive strain increases (λ ~ 0.94 to 0.92), a gradual softening is observed. At this stage, a significant number of fibers undergo large bending deformations, thus reducing the number of load sustaining members. Foams also exhibit this type of behavior, which is associated with strain localization in a band that traverses the sample. The band then moves across the sample leading to full compaction of the foam and to a characteristic plateau in the stress-strain curve [2]. In mycelium, as well as in our microscale models, strain localization occurs in sub-regions of the model which, initially, do not percolate. This is due to the more irregular geometry of the fibrous network compared to the foams with periodic or quasi-periodic microstructure. Localization in a major band eventually happens in the present microscale models too, but the resulting band does not move across the sample as global deformation proceeds. Fig. 6 shows the deformed configurations of a network of density $\rho_m = 17.1$ kg/m^3 at three strain levels $\lambda = 0.99$,0.95 and 0.85. The von Mises stress contours are overlaid in order to show the degree of stress (and hence strain) heterogeneity. Heterogeneity is observed even in the linear regime, for stretch ratios close to 1, e.g. $\lambda = 0.95$, and it becomes pronounced at $\lambda = 0.85$.

3.2. Mesoscale density distribution

The mesoscale model is a continuum model whose size is comparable with that of mycelium samples used in experiments. Density variability is incorporated in this model at a length scale larger than the microscale model size (L) by introducing subdomains. Each subdomain is assigned a density, sampled from a calibrated distribution, and the constitutive behavior is derived from a microscale network model of corresponding density.

In general, elastic properties (e.g. elastic moduli) of network based materials are explicit functions of density. Therefore, density variability in the material has a unique correlation with local moduli variation which in turn affects the local strain field especially in the small strain regime. Since density variability on the microscale could not be measured directly in the experimental samples, the local strain field (on the sample surfaces) estimated from digital image correlation (DIC) was used as an indirect measure of the random density field. Specifically, a trial-error based inverse problem is formulated where the density/elastic moduli distribution of the mesoscale subdomains is tuned to achieve comparable strain distribution as obtained experimentally with DIC. We further conjecture that the spatial correlation length of the strain field is identical to that of the underlying density/elastic moduli fluctuations. The size of the individual subdomain is set equal to this characteristic length and the size of the mesoscale model is taken 20 times the size of an individual subdomain in order to eliminate size effects of the continuum mesoscale homogenization. The mesoscale model contains 8000 subdomains.

The distribution of mesoscale density is represented with a beta distribution. The beta distribution can accommodate a wide variety of distribution shapes and thereby, it facilitates the calibration of distribution parameters especially in absence of prior knowledge on the actual distribution. The distribution is defined as:

$$P(\rho_m|a,b) = \frac{\rho_m{}^{a-1}(1-\rho_m)^{b-1}}{B(a,b)}, \tag{2}$$

where B is the Beta function, $B(a,b) = \Gamma(a)\Gamma(b)/\Gamma(a+b)$, with Γ being the Gamma function and (a,b) shape parameters. The mean (μ) and variance (σ^2) of the distribution are given as $\mu = a/(a+b)$ and $\sigma^2 = ab/[(a+b)^2(a+b+1)]$, respectively. The moments (μ, σ^2) and hence, the shape parameters (a,b) are determined by the iterative search method discussed above. The search begins with an initial guess of the shape parameters (a,b) and the mesoscale model is simulated for this initial guess. The predicted strain distribution is compared to the DIC measurements, the initial guess is updated accordingly and the search is repeated until a satisfactory agreement between the statistics of model predictions and DIC measurements is obtained. We note that the mean of the distribution is equal to the actual sample mass density ($\mu = \rho_s$) and a coefficient of variance of 0.48 ($\sigma/\mu = 0.48$) provides a density distribution representative of actual mycelium samples.

Fig. 7 shows the distribution of mesoscale density inferred through the procedure described above for the sample of average (macroscopic) density $\rho_s = 34$ kg/m^3. The distribution is further mapped to a set of 10 delta functions (shown by vertical bars in Fig. 7) equally spaced in the range of densities $\rho_m = 8$ kg/m^3 to $\rho_m = 78$ kg/m^3. For samples of other mean densities ρ_s (in the experimental range of 8 to 78 kg/m^3), the distribution is kept the same, while the mean is adjusted accordingly.

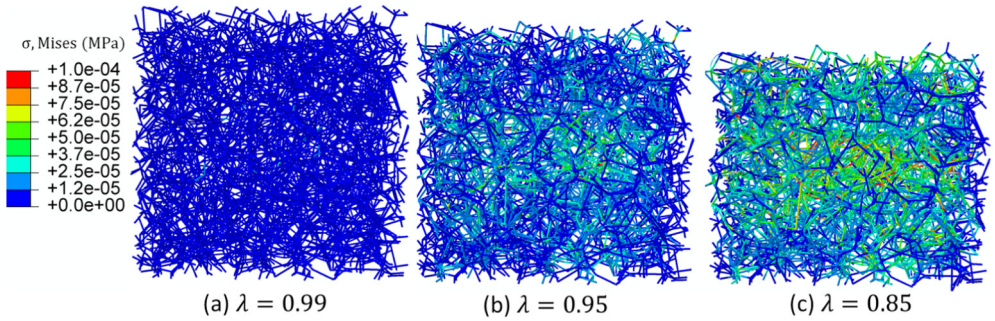

Fig. 6. Deformed configurations of a micro-scale network model ($\rho_m = 16.9$ kg/m^3) with von Mises stress contours corresponding to applied stretch ratio values of (a) $\lambda = 0.99$, (b) $\lambda = 0.95$ and (c) $\lambda = 0.85$.

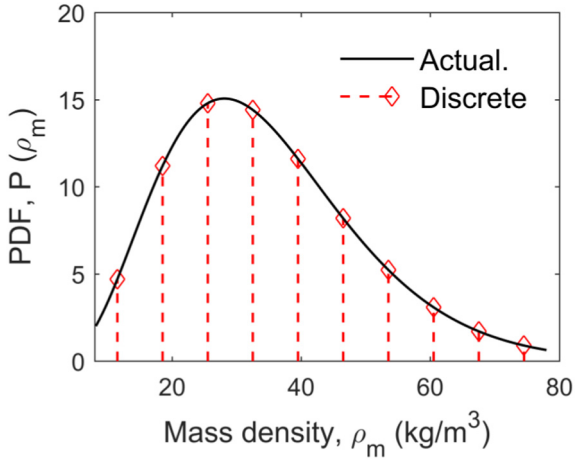

Fig. 7. Representative mesoscale density distribution for a sample of average density ρ_s = 34 kg/m^3. The black line represents the actual distribution and the vertical bars indicate the corresponding approximation.

The mechanical behavior of models of all ten densities defining the discrete distribution in Fig. 7 is evaluated using microscale models.

3.3. Constitutive representation of microscale model behavior

The microscale model stress-strain response is described in the mesoscale continuum model using hyperelastic constitutive equations. These are defined starting from a scalar strain energy density function, $W(\mathbf{C})$, written in terms of the right Cauchy-Green deformation tensor ($\mathbf{C}$). The nominal stress, $\mathbf{S}$, is obtained as $\mathbf{S} = 2\mathbf{F}\partial W/\partial\mathbf{C}$, where $\mathbf{F}$ is the deformation gradient and $\mathbf{C} = \mathbf{F}^T\mathbf{F}$. Alternately, for an isotropic solid the strain energy density is expressed in terms of the principal stretches ($\lambda_1, \lambda_2, \lambda_3$) and the nominal principal stress components become $S_{ii} = \partial W/\partial\lambda_i$. Here, we consider a strain energy function for compressible hyperelastic materials proposed by Storakes [29]:

$$W = W(\mathbf{C}) = W(\lambda_1, \lambda_2, \lambda_3) = \sum_{i=1}^{N} \frac{2\mu_i}{\alpha_i^2}\left(\lambda_1^{\alpha_i} + \lambda_2^{\alpha_i} + \lambda_2^{\alpha_i} - 3 + \frac{1}{\beta_i}\left(J^{-\alpha_i\beta_i} - 1\right)\right) \quad (3)$$

where μ_i, α_i and β_i are material coefficients. J is the Jacobian $J = \det\mathbf{F}$ and N is the number of terms in the series. The coefficients, β_i, determines the degree of compressibility, and is related to the Poisson ratio (ν_i) as $\nu_i/(1-\nu_i)$. All terms, β_i, are considered identical and correspond to a global Poisson ratio, ν. The small strain shear modulus, μ_0, is defined as $\mu_0 = \sum_{i=1}^{N}\mu_i$ and the corresponding bulk modulus, K_0, is obtained as $K_0 = \sum_{i=1}^{N} 2\mu_i(\beta_i + 1/3)$. Finally, if the material is loaded uniaxially, the nominal stress in the loading direction, S_L, is:

$$S_L = \frac{\partial W}{\partial\lambda_L} = \frac{2}{\lambda_L}\sum_{i=1}^{N}\frac{\mu_i}{\alpha_i}\left(\lambda_L^{\alpha_i} - J^{\alpha_i\beta_i}\right) \quad (4)$$

where the coefficients (μ_i, α_i *and* β_i) need to be determined by fitting the stress-strain curves obtained from the microscale model. Material coefficients are determined by a nonlinear least-squares fit methods based on Marquard-Levenberg algorithm [30] by minimizing relative error in stress. A fit of expression (4) with three terms in the sum, $N = 3$, provides a good approximation of the stress-strain response of various network densities with relative error <5% for all densities. Fig. 4 shows the fits obtained using Eq. (4) for four representative network densities. To represent the entire density distribution as shown in Fig. 7, ten similar network densities (corresponding to the vertical bars in Fig. 7) are considered and the resulting material parameters are shown in Table A1. The hyperelastic formulation discussed here is implemented using the HYPERFOAM material model available in the commercial finite element package Abaqus.

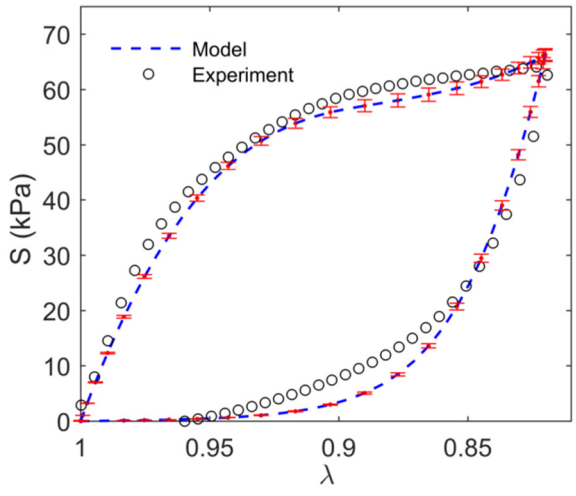

Fig. 8. Comparison of model response (dotted line) and experimental stress-strain curve (symbols) for sample density (ρ_s = 34 kg/m^3) under single compression cycle. Error bars indicate the range of three mesoscale model realizations.

3.4. Damage model

Mycelium exhibits a marked hysteresis and stress softening effect under cyclic compression, which are primarily caused by damage accumulation within the material. However, the microscale network model does not include any damage component. In order to account for hysteresis and stress softening, a phenomenological damage model is used. For this purpose, the model proposed by Ogden and Roxburgh [31] was used. In this representation, the strain energy density is rendered as a function of a damage variable, η, i.e. $W\sim(\mathbf{F},\eta) = \eta W(\mathbf{F}) + \phi(\eta)$. Here, $\phi(\eta)$ is a continuous damage function. The damage variable, η, varies continuously during deformation as described by:

$$\eta = 1 - \frac{1}{r}\,\mathrm{erf}\left(\frac{W\sim^{m} - W}{m + \beta W\sim^{m}}\right) \quad (5)$$

where $W\sim^{m}$ is the maximum value of $W\sim$ at a material point for a given deformation level, (r, m, β) are material parameters and erf(.) is the error function. The damage variable varies in the interval $0 < \eta \le 1$. In particular, during initial loading, η remains constant ($\eta = 1$) and the damage function satisfies, $\phi(1) = 0$. On the other hand, when the load is removed completely ($W = 0$), η reaches its minimum, defined as $\eta_m = 1 - \frac{1}{r}\,\mathrm{erf}\left(\frac{W\sim^{m}}{m + \beta W\sim^{m}}\right)$. For other values of W, η varies monotonically between 1 and η_m. These constants do not have physical significance; rather they are used to control damage evolution by calibrating with respect to experimental damage accumulation or dissipation curves, similar to Fig. 2. The experimental results (Fig. 2(a)) indicate that the damage is largely controlled by the maximum stress/strain reached and does not vary significantly with the mean sample density. Therefore, we observe that a single set of damage coefficients (r,m, β) is adequate to predict damage behavior of mycelium of various mean densities.

4. Calibration and validation

In this section, the calibration and validation of the multiscale model is presented. The model has two calibration components, namely the mesoscale density distribution and the damage parameters (r, m, β) of Eq. (5). The density distribution is calibrated using an iterative procedure by comparing model predicted strain distribution and DIC

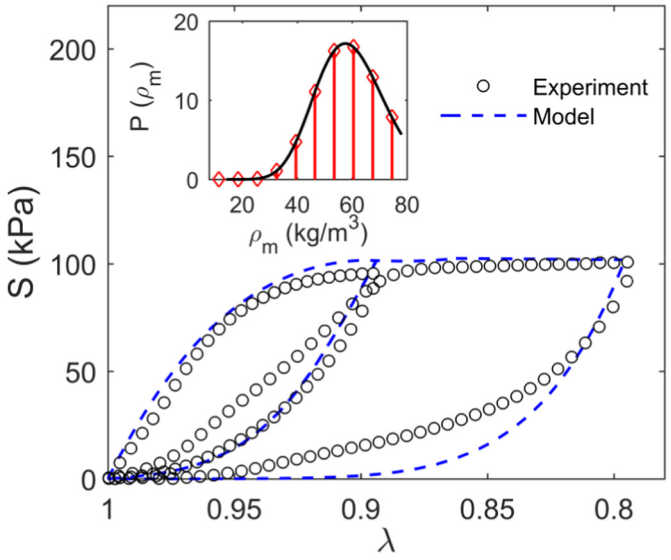

Fig. 9. Comparison of model prediction (dotted line) and experiments (symbols) for sample density ($\rho_s = 59$ kg/m^3) under two compression cycles. The inset shows the density distribution used.

measurements, as discussed in Section 3.2. On the other hand, the damage parameters (r, m, β) are calibrated by comparing the model predicted stress-strain response with the experimental response. In this case, the stress-strain curve of a single compression cycle for sample density ($\rho_s = 34$ kg/m^3) is used (black curve in Fig. 2(a)). Finally, the model is validated by predicting the experimental stress-strain response for multiple compression cycles (Fig. 2(b)).

Fig. 8 compares the response of the multiscale model with the experimental stress-strain curves in Fig. 2(a), corresponding to a sample of density, $\rho_s = 34$ kg/m^3, which is subjected to a single compression cycle. The model response is the average of three realizations of the multiscale model, and the error bars represent the range of the respective replicas. The unloading branch is matched by fitting damage parameters- $r = 1.01$, $m = 0.005$ and $\beta = 0.1$ in Eq. (5). It is to be noted that the loading branch of Fig. 8 is a model prediction since the density distribution has already been defined as described in Section 3.2. In this case, the density distribution is the same as shown in Fig. 7.

In Fig. 9, the model prediction is validated with respect to the experimental results in Fig. 2(b) corresponding to a sample of mean density $\rho_s = 59$ kg/m^3. Here, the experimental curve is obtained from the primary loading-unloading paths. The density distribution is shown in the inset and the calibrated damage parameters ($r = 1.01$,$m = 0.005$, β=0.1) are used. The multiscale model is able to predict the highly non-linear behavior of mycelium accurately, except for the residual strain. In the absence of accurate elastic-plastic properties for individual hyphae, the residual strain or permanent set cannot be captured. Further, the predicted unloading and reloading curves are identical, whereas the respective paths are slightly different in experiment. This is most likely due to viscoelastic recovery of mycelium after unloading. Since no viscoelastic component is included in the model, the model cannot account for such recovery as seen in experiment. This difference is considered unimportant for the purpose of the developed model.

5. Conclusion

We presented a multiscale model to describe the non-linear mechanical behavior of mycelium under cyclic compression loading. The model efficiently integrates a micro-scale random fiber network model characterizing the fibrous microstructure of mycelium, with a continuum model that takes into account density fluctuations. In addition, an empirical damage model is incorporated to account for stress softening.

We demonstrated the validity of the developed model by comparison with experimental results from multiple compression cycles. The model captures the primary loading curve and unloading accurately.

The model can be easily generalized to predict complex three-dimensional deformation of other similar materials such as polymeric foams, soft tissue or hydrogels, where consideration of density fluctuation and network-like microstructure is important. Its use in the context of other types of networks is facilitated by the fact that parameters of fitted hyperelastic models with damage are presented for a broad range of network densities (Appendix A). This allows using only the less complex and less computationally expensive mesoscale model in any future applications. The model can be used to design mycelium and mycelium-based composites for a broad range of applications.

Author contribution statement

M.R. Islam performed the testing and numerical analysis, G. Tudryn provided expertise related to material processing and microstructure, R. Bucinell contributed to testing, L.S. Schadler and R.C. Picu developed the plan of work, contributed technically to all components of the work and supervised the project.

Acknowledgement

This material is based on work supported by the US National Science Foundation (NSF) under Grant no. CMMI 1362234.

Appendix A

Hyperelastic model parameters, as defined by Eq. (3), are summarized for ten network densities in Table A1. These parameter sets are used to define the constitutive behavior of each sub-domain of the continuum mesoscale model according to the density distribution of Eq. (2). The values of μ_i are in MPa, while α_i and β_i are dimensionless.

Table A1
Summary of hyperelastic model parameters for ten different network densities.[1,2]

ρ_m (kg/m^3)	μ_1	α_1	μ_2	α_2	μ_3	α_3	β
10.3	0.781596	6.56724	−0.29858	4.46147	−0.39316	4.49773	0.3793
16.9	−30.069	−1.68619	16.554	−0.77516	13.6929	−2.52915	0.3793
25.3	1.9383	7.57854	1.64607	7.57949	−3.25804	5.65142	0.3793
36.1	−46.6449	−1.49798	25.9885	−0.52104	21.0135	−2.39752	0.3793
39	3.82235	7.35262	2.03493	7.3551	−5.32076	5.56589	0.3793
47.5	3.14686	5.06527	−1.27358	2.55403	−1.29612	2.47474	0.3793
53.2	5.19417	7.35262	2.76526	7.3551	−7.23036	5.56589	0.3793
61.5	3.97498	5.06526	−1.60873	2.55404	−1.6372	2.47474	0.3793
67.3	6.56622	7.35262	3.4957	7.3551	−9.14027	5.56589	0.3793
76.1	7.35025	7.35262	3.9131	7.3551	−10.2316	5.56589	0.3793

[1] Values of μ_i are in (MPa), α_i and β_i are dimensionless.
[2] $\beta = \beta_1 = \beta_2 = \beta_3$.

References

[1] M. Islam, G. Tudryn, R. Bucinell, L. Schadler, R. Picu, Morphology and mechanics of fungal mycelium, Sci. Rep. 7 (1) (2017), 13070.
[2] L.J. Gibson, M.F. Ashby, Cellular Solids: Structure and Properties, Cambridge University Press, 1999.
[3] A. Dorfmann, R.W. Ogden, A constitutive model for the Mullins effect with permanent set in particle-reinforced rubber, Int. J. Solids Struct. 41 (7) (2004) 1855–1878.
[4] L. Mullins, Softening of rubber by deformation, Rubber Chem. Technol. 42 (1) (1969) 339–362.
[5] L. Zhao, D. Schaefer, H. Xu, S.J. Modi, W.R. LaCourse, M.R. Marten, Elastic properties of the cell wall of *Aspergillus nidulans* studied with atomic force microscopy, Biotechnol. Prog. 21 (1) (2005) 292–299.
[6] G. Michalenko, H. Hohl, D. Rast, Chemistry and architecture of the mycelial wall of Agaricus bisporus, Microbiology 92 (2) (1976) 251–262.
[7] I. Joffe, H. Hepburn, Observations on regenerated chitin films, J. Mater. Sci. 8 (12) (1973) 1751–1754.
[8] S. Ifuku, H. Saimoto, Chitin nanofibers: preparations, modifications, and applications, Nanoscale 4 (11) (2012) 3308–3318.
[9] Y. Fan, H. Fukuzumi, T. Saito, A. Isogai, Comparative characterization of aqueous dispersions and cast films of different chitin nanowhiskers/nanofibers, Int. J. Biol. Macromol. 50 (1) (2012) 69–76.
[10] N. Ezekiel Mushi, N. Butchosa, Q. Zhou, L.A. Berglund, Nanopaper membranes from chitin–protein composite nanofibers—structure and mechanical properties, J. Appl. Polym. Sci. 131 (7) (2014).
[11] I. Ofenbeher-Miletić, D. Stanimirović, S. Stanimirović, On determination of chitin content in mushrooms, Plant Foods Hum. Nutr. 34 (3) (1984) 197–201.
[12] R.R. Naik, S. Singamaneni, Introduction: bioinspired and biomimetic materials, ACS Publications2017.
[13] M.R. Islam, R.C. Picu, Effect of network architecture on the mechanical behavior of random fiber networks, J. Appl. Mech. 85 (8) (2018), 081011.
[14] S. Gaitanaros, S. Kyriakides, A.M. Kraynik, On the crushing of polydisperse foams, Eur. J. Mech. A. Solids 67 (2018) 243–253.
[15] O. Gültekin, G.A. Holzapfel, A brief review on computational modeling of rupture in soft biological tissues, Advances in Computational Plasticity, Springer 2018, pp. 113–144.
[16] R. Rivlin, Large elastic deformations of isotropic materials IV. Further developments of the general theory, Philos. Trans. R. Soc. Lond. A 241 (835) (1948) 379–397.
[17] E.M. Arruda, M.C. Boyce, A three-dimensional constitutive model for the large stretch behavior of rubber elastic materials, J. Mech. Phys. Solids 41 (2) (1993) 389–412.
[18] R. Ogden, Large deformation isotropic elasticity-on the correlation of theory and experiment for incompressible rubberlike solids, Proc. R. Soc. Lond. A (1972) 565–584.
[19] T. Lu, J. Wang, R. Yang, T. Wang, A constitutive model for soft materials incorporating viscoelasticity and Mullins effect, J. Appl. Mech. 84 (2) (2017), 021010.
[20] B.H. Kaye, A Random Walk Through Fractal Dimensions, John Wiley & Sons, 2008.
[21] S. Kale, M. Ostoja-Starzewski, Morphological study of elastic-plastic-brittle transitions in disordered media, Phys. Rev. E 90 (4) (2014), 042405.
[22] R. Picu, S. Sorohan, M. Soare, D. Constantinescu, Towards designing composites with stochastic composition: effect of fluctuations in local material properties, Mech. Mater. 97 (2016) 59–66.
[23] L. Huyse, M.A. Maes, Random field modeling of elastic properties using homogenization, J. Eng. Mech. 127 (1) (2001) 27–36.
[24] M.D. Abràmoff, P.J. Magalhães, S.J. Ram, Image processing with ImageJ, Biophoton. Int. 11 (7) (2004) 36–42.
[25] A. Version, 6.13, Analysis User's Manual. , Dassault Systems Simulia Corp., Providence, RI, 2013.
[26] M. Islam, G.J. Tudryn, C.R. Picu, Microstructure modeling of random composites with cylindrical inclusions having high volume fraction and broad aspect ratio distribution, Comput. Mater. Sci. 125 (2016) 309–318.
[27] A.I. Abd El-Rahman, C.L. Tucker, Mechanics of random discontinuous long-fiber thermoplastics. Part II: direct simulation of uniaxial compression, J. Rheol. 57 (5) (2013) 1463–1489.
[28] A. Shahsavari, R. Picu, Size effect on mechanical behavior of random fiber networks, Int. J. Solids Struct. 50 (20) (2013) 3332–3338.
[29] B. Storåkers, On material representation and constitutive branching in finite compressible elasticity, J. Mech. Phys. Solids 34 (2) (1986) 125–145.
[30] E. Twizell, R. Ogden, Non-linear optimization of the material constants in Ogden's stress-deformation function for incompressinle isotropic elastic materials, ANZIAM J. 24 (4) (1983) 424–434.
[31] R. Ogden, D. Roxburgh, A pseudo–elastic model for the Mullins effect in filled rubber, Proc. R. Soc. Lond. A (1999) 2861–2877.